

Efficient generation of non-classical photon pairs in a hot atomic ensemble

Chengyuan Wang (王程远), Yan Gu (辜 滢), Ya Yu (余 娅), Dong Wei (卫 栋),
Pei Zhang (张 沛), Hong Gao (高 宏)*, and Fuli Li (李福利)

Shaanxi Key Laboratory of Quantum Information and Quantum Optoelectronic Devices, School of Science, Xi'an Jiaotong University, Xi'an 710049, China

*Corresponding author: honggao@xjtu.edu.cn

Received March 31, 2018; accepted June 6, 2018; posted online July 16, 2018

We demonstrate the generation of non-classical photon pairs in a warm ^{87}Rb atomic vapor cell with no buffer gas or polarization preserving coatings via spontaneous four-wave mixing. We obtain the photon pairs with a $1/e$ correlation time of 40 ns and the violation of Cauchy–Schwartz inequality by a factor of 23 ± 3 . This provides a convenient and efficient method to generate photon pair sources based on an atomic ensemble.

OCIS codes: 270.5290, 190.4223.

doi: 10.3788/COL201816.082701.

Entangled photon pairs are vital tools in the research of quantum information, quantum computation, quantum cryptography, and quantum imaging^[1]. The most common method to generate paired photons is spontaneous parametric down conversion (SPDC) using nonlinear crystals^[2,3]. Photons generated in this way have limited applications in an atomic-based quantum network because of their intrinsic broadband linewidth ($\sim\text{THz}$), low spectral brightness, and short coherence time that is beyond the resolution of photodetectors. Various techniques, such as cavity assisted SPDC^[4,5] and spontaneous four-wave mixing (SWMF) based on atomic ensembles^[6–9], have been put forward to narrow down the linewidth of photon pairs in recent years. Photon pairs generated in cold atomic ensembles can be manipulated to have a very long coherence time in the presence of electromagnetically induced transparency (EIT)^[10–12]. In spite of the distinct advantages of cold atoms in generating photon pairs, the system is complicated and needs bulky light and magnetic fields. Many researchers have made attempts to produce non-classical photon pairs with hot atomic ensembles in recent years^[13–15], but the outcomes were not that satisfactory because of the short coherence time or low contrast ratio. Recently, Du *et al.* realized sub-natural linewidth and high spectral brightness photon pairs with a paraffin-coated hot atomic vapor cell^[16,17]. Podhora *et al.* realized nonclassical correlated photon pairs by using a single laser in a retro-reflected configuration and a 7.5 cm long cylindrical glass cell that does not contain any atomic polarization preserving coatings or buffer gas^[18]. The non-classicality is satisfactory, but the coherence time is limited to less than 5 ns in this configuration.

In this Letter, we attempt to generate narrowband non-classical photon pairs in a ^{87}Rb atomic vapor cell that has no buffer gas or any polarization preserving coatings via SFWM in continuous-wave operation mode. The atomic cell used in our experiment (diameter and length of 25.4 and 50 mm) is commonly exploited for many

atomic-based experiments and is facilely fabricated. By using the similar setup as in Ref. [16] and carefully suppressing the fluorescence noise, we produce the non-classical photon pairs at a rate of 2100 s^{-1} with the $1/e$ correlation time of 40 ns, which exceeds the natural lifetime of Rb $5P$ excited states (26.5 ns). Due to the greatly simplified experimental requirements, our results may provide a convenient and efficient method to generate photon pair sources based on the atomic ensemble.

The experimental setup and corresponding energy diagram are schematically illustrated in Figs. 1(a) and 1(b), respectively. The pump beam (ω_p) and the coupling beam (ω_c) both have vertical polarization counter propagating through the vapor cell. The pump beam is resonant with the ^{85}Rb transition $|5S_{1/2}, F=2\rangle \rightarrow |5P_{3/2}, F=3\rangle$,

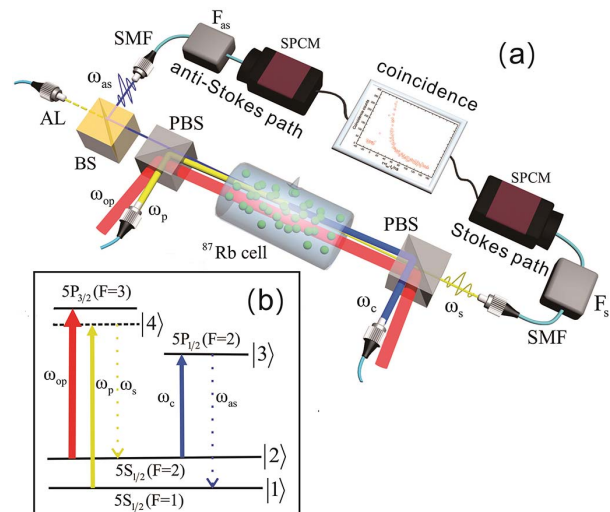


Fig. 1. (a) Sketch of the experimental setup and (b) the energy diagram of SFWM. (PBS, polarizing beam splitter; BS, beam splitter; SMF, single mode fiber; F_s and F_{as} , filters in the Stokes path and anti-Stokes path; SPCM, single-photon counting module; AL, auxiliary laser.)

which is red detuned from the ^{87}Rb transition $|5S_{1/2}, F=1\rangle \rightarrow |5P_{3/2}, F=2\rangle$ by 2.7 GHz. The coupling beam is resonant with the ^{87}Rb transition $|5S_{1/2}, F=2\rangle \rightarrow |5P_{1/2}, F=2\rangle$. To avoid the uncorrelated anti-Stokes noise from on-resonance scattering of the coupling beam, an additional vertically polarized optical pumping beam with the frequency $|5S_{1/2}, F=2\rangle \rightarrow |5P_{3/2}, F=3\rangle$ of ^{87}Rb is used. The phase-matched horizontally polarized Stokes (780 nm, ω_s) and anti-Stokes (795 nm, ω_{as}) photons are spontaneously generated in the cell with the frequency shown in Fig. 1(b) and are collected with an angle of 1° relative to the pump and coupling beams on the backward direction by two single mode fibers. This configuration makes it easier to filter the generated photons from the strong experimental lasers in space and polarization. Besides, because of the non-degenerated features, the best phase matching (PM) direction is not exactly collinear between the Stokes and anti-Stokes photons. In order to find the best PM angle, an auxiliary laser (AL) beam is utilized to simulate the Stokes field, and then a four-wave mixing signal is generated. This beam and the four-wave mixing signal are carefully coupled into two single mode fibers, which are used to collect Stokes and anti-Stokes photons afterwards.

The collected Stokes and anti-Stokes photons are then sent into single photon counting modules (Perkin-Elmer SPCM-AQR-14), and the time-resolved coincidences are recorded using a time digitizer (SPC-630, 1 ns bin width with a total of 256 bins) after passing through some frequency filters. The filters in the Stokes path are composed of a 780 nm optical filter (10 nm bandwidth) and two narrowband etalon filters (500 MHz bandwidth, total 50 dB extinction ratio) in series, and the total transmission efficiency is 30%. The filters in the anti-Stokes path are composed of a 795 nm optical filter (10 nm bandwidth) and a narrowband etalon filter (500 MHz bandwidth, 25 dB extinction ratio), and the total transmission efficiency is 40%.

There has been a study in generating non-classical photon pairs in a hot atomic ensemble with two level resonant lasers^[13], but the contrast ratio is relatively low. This probably results from the on-resonance fluorescence noise that has the same frequency as the Stokes signal. In order to confirm this noise and suppress it, the frequency component of the fluorescence is measured. We remove the second etalon and record the fluorescence intensity by scanning the first etalon in the presence of the pump beam and coupling beam in the Stokes path. The powers of the pump beam and coupling beam are 20 mW and 27 mW with the vapor temperature kept at 40°C . The null point of the etalon detuning in Fig. 2 is calibrated at the ^{87}Rb transition $|5S_{1/2}, F=2\rangle \rightarrow |5P_{3/2}, F=2\rangle$. As can be seen in Fig. 2(a), the fluorescence intensity near the null point is much higher than the adjacent Stokes signal. To get a high contrast ratio, the Stokes signal should be kept away from the on-resonance fluorescence in the experiment. Then, we fix the first etalon at -2.7 GHz detuned from the null point and scan the second etalon. As shown in

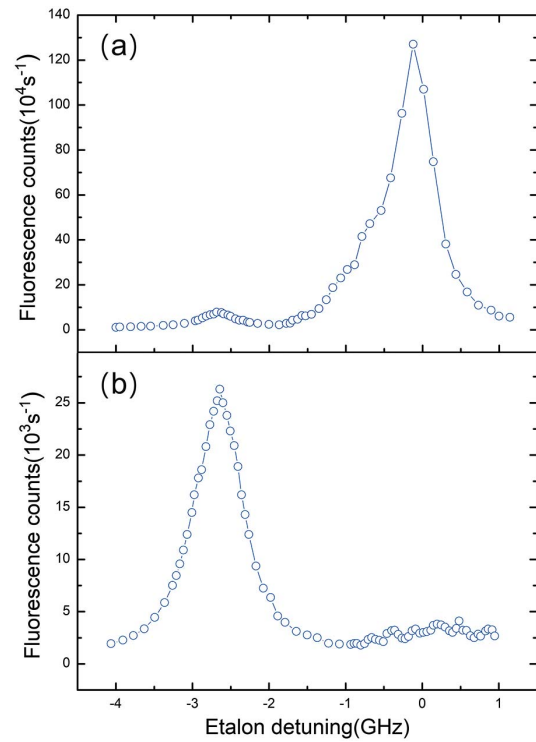


Fig. 2. Spectral scan of the fluorescence in the Stokes path. (a) Scan the first etalon with the second etalon removed. The strong peak near the null point is the on-resonance fluorescence noise, and the weak peak near the -2.7 GHz detuning is the Stokes signal. (b) Scan the second etalon. Clearly, the fluorescence noise is significantly filtered. (The solid lines in all of the figures are guides for the eyes.)

Fig. 2(b), it can be clearly seen that the fluorescence background is largely filtered.

The fluorescence in the anti-Stokes path mainly comes from the uncorrelated atoms in state $|2\rangle$, which can be suppressed by pumping these atoms to state $|1\rangle$ with an additional optical pumping beam. Figure 3 shows the measured relationship between the fluorescence intensity and the power of the optical pumping beam with only the coupling beam on. As the optical pumping beam power increases from 0 to 170 mW, the detected fluorescence

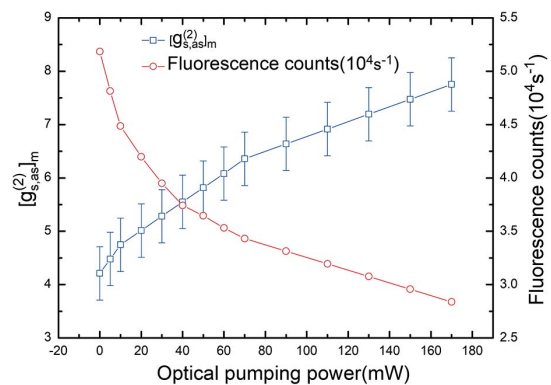


Fig. 3. Fluorescence intensity and cross correlation function versus the optical pumping beam power.

drops from 52,000 per second to 27,000 per second. Then, we switch on the pump beam and measure the maximum value of cross correlation function $[g_{s,as}^{(2)}]_m$ (computational formula is shown below) as we increase the power of the optical pumping beam. As can be seen, the $[g_{s,as}^{(2)}]_m$ rises from 4.2 to 7.7. This means that the optical pumping beam is helpful in diminishing the uncorrelated anti-Stokes fluorescence.

A classical light field is bounded by the Cauchy–Schwartz inequality $[g_{s,as}^{(2)}(\tau)]^2/[g_{s,s}^{(2)}(0)g_{as,as}^{(2)}(0)] \leq 1$, while a quantum field violates it. In the ideal case, the autocorrelation functions should be $g_{s,s}^{(2)}(0) = g_{as,as}^{(2)}(0) = 2$, so the non-classical property is mostly evaluated by the cross correlation function $g_{s,as}^{(2)}(\tau)$. In the following parts of the experiment, we demarcate the non-classical property of the photon pairs by measuring the maximum value $[g_{s,as}^{(2)}]_m$ of $g_{s,as}^{(2)}(\tau)$.

Figure 4(a) shows the time-resolved coincidence versus time delay τ recorded by our coincidence board after the filtering systems. The powers of the pump, coupling, and optical pumping beams are 20, 29, and 170 mW, respectively, and the vapor temperature is 40°C. From the data, we can get the cross correlation function $g_{s,as}^{(2)}(\tau)$ with the maximum value $[g_{s,as}^{(2)}]_m = 8 \pm 0.5$. The autocorrelation functions of Stokes and anti-Stokes photons measured in our experiment are $g_{s,s}^{(2)}(0) = 1.77$ and $g_{as,as}^{(2)}(0) = 1.58$. With the above values, we obtain the violation of Cauchy–Schwartz inequality by a factor of 23 ± 3 , which verifies the non-classical property of the photon pairs. From the data, we can also get that the photon pair’s generation rate is about 2100 s^{-1} (the total collection efficiency is about 10%), and the $1/e$ correlation time is about 40 ns, which exceeds the natural lifetime of the Rb 5P excited states. This means that the electromagnetically induced transparency effect created by the on-resonance coupling beam is helpful for prolonging the photon coherence time and narrowing the bandwidth of the photon pairs in this

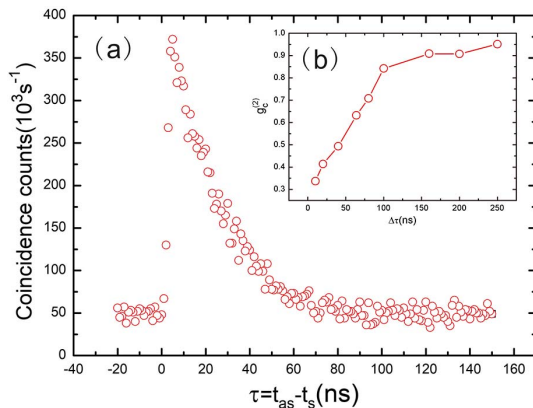


Fig. 4. (a) Photon pairs coincidence counts with 90 s collection time. (b) The conditional autocorrelation function $g_c^{(2)}$ of heralded single anti-Stokes photons with 35 min acquisition time.

kind of vapor cell. The limited optical depth (OD) of the hot atomic vapor cell and the high spin relaxation rate of the atomic ground state resulted from the fast atomic motion and drastic collisions are the main limiting factors that affect the correlation time of paired photons. If we can get a high OD and at the same time keep a low spin relaxation rate, a longer coherence time is expected to be obtained. We also measure the heralded single photon property of the anti-Stokes field with the method in Refs. [19,20]. A fiber beam splitter is used to separate the anti-Stokes field into two paths (marked as as1 and as2 below). The conditional autocorrelation function $g_c^{(2)} = P_{s,as1,as2}/(P_{s,as1} \cdot P_{s,as2})$ is measured as a function of the coincidence window width $\Delta\tau$ with 35 min acquisition time.

As can be seen in Fig. 4(b), $g_c^{(2)}$ is below the two-photon threshold 0.5 with the coincidence window less than 50 ns.

Next, we characterize the non-classical property of the photon pairs by changing the pump beam power, the coupling beam power, as well as the vapor’s temperature. In Fig. 5(a), the coupling power is fixed to 28 mW, and the pump power is changed from 4 to 20 mW. While in Fig. 5(b), the pump power is set at 20 mW, and the coupling power ranges from 4 to 29 mW. The temperature of the vapor cell here is kept at 40°C. Both results show that the $[g_{s,as}^{(2)}]_m$ increases continuously with the increase of the pump and coupling beam power until they get to the maximum output power of our lasers. Generally, at a certain

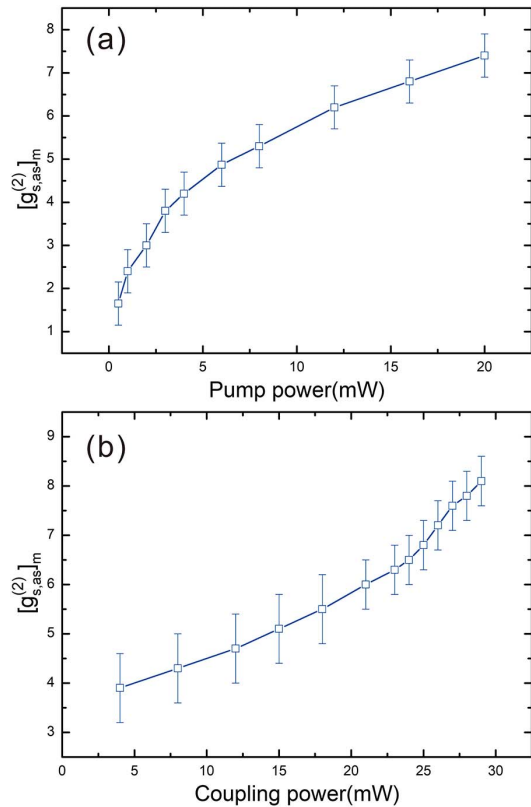


Fig. 5. Cross correlation function as a function of (a) pump power and (b) coupling power.

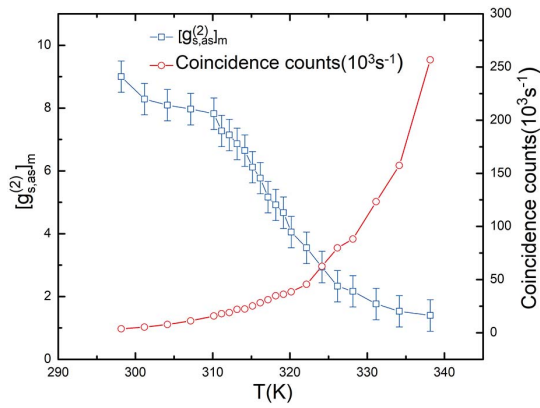


Fig. 6. Cross correlation function and coincidence counts versus the vapor temperature. The power of pump, coupling, and optical pumping beams are 20, 29, and 170 mW, respectively.

atomic density, the cross correlation function increases with pump beam power because the exciting rate of the Stokes photons grows faster than the uncorrelated noise photons. This trend tends to saturate and then drop because the probability of exciting multiple photons comes out with high pump beam power. The multiple photon process contributes to the uncorrelated photon noise, which eventually degrades the cross correlation function. On the other hand, as an increment of the coupling power, the cross correlation function increases due to the enhanced retrieving efficiency of the anti-Stokes photons. Increasing the pump and coupling beam power and seeking a more effective way to suppress and filter the uncorrelated photon noise can further promote the cross correlation function before multiple photon excitation dominates.

Figure 6 shows the dependence of $[g_{s,as}^{(2)}]_m$ and coincidence rate on the temperature of our atomic vapor cell. The generation rate rises exponentially, while $[g_{s,as}^{(2)}]_m$ decreases dramatically with the increase of vapor temperature. This is because the uncorrelated fluorescence plays a dominant role in the coincidence count with the high atomic density and drastic atomic thermal motion. So, one has to make a compromise in getting a higher generation rate while keeping the non-classical property by increasing the vapor cell's temperature. We think that narrower bandwidth etalon filters can further suppress the fluorescence noise and enhance the signal to noise ratio of the anti-Stokes field.

Before drawing conclusions, we should address that although our experimental results are not as good as those in the paraffin-coated cell, it indicates that the vapor cell without the polarization preserving coatings or buffer gas is also capable of generating sub-natural linewidth photon pairs with a high generation rate. Besides, this kind of cell is more facilely fabricated and easy to maintain; hence, they are more commonly used in experiments. In addition, our experimental setup does not contain a magnetic shield and complicated heating systems, and there is no need for a complex time sequence as in the cold atom systems, so

the experimental requirements are greatly simplified. This provides a miniaturized and convenient method in generating narrowband photon pairs and may have extensive applications in an atomic-memory-based quantum network.

In conclusion, we demonstrate the generation of non-classical photon pairs in a warm ^{87}Rb atomic vapor cell via SFWM. The photon pair's generation rate is about 2100 s^{-1} , and the $1/e$ correlation time is 40 ns. The fluorescence noise in the Stokes path is decreased by detuning the pump beam away from the resonant transition and by using optical filter systems. An optical pumping beam is used to suppress the uncorrelated photon noise in the anti-Stokes path. With these measures, we get the violation of the Cauchy-Schwartz inequality by a factor of 23 ± 3 . The generation rate and the non-classical property can be further enhanced by increasing the laser power and optimizing the spatial profile of the optical pumping beam.

This work was supported by the Fundamental Research Funds for the Central Universities and the National Natural Science Foundation of China (Nos. 11774286, 11374238, 11574247, 11374008, and 11534008).

References

1. D. Bouwmeester, A. Ekert, and A. Zeilinger, *The Physics of Quantum Information* (Springer-Verlag, 2000).
2. M. Xia, J. Li, Y. Hu, W. Sheng, D. Gao, W. Pang, and X. Zheng, *Chin. Opt. Lett.* **13**, 113001 (2015).
3. D. A. Antonosyan, A. S. Solntsev, and A. A. Sukhorukov, *Photon. Res.* **6**, A6 (2018).
4. Z. Y. Ou and Y. J. Lu, *Phys. Rev. Lett.* **83**, 2556 (1999).
5. C. E. Kuklewicz, F. N. C. Wong, and J. H. Shapiro, *Phys. Rev. Lett.* **97**, 223601 (2006).
6. L. M. Duan, M. D. Lukin, J. I. Cirac, and P. Zoller, *Nature* **414**, 413 (2001).
7. A. Kuzmich, W. P. Bowen, A. D. Boozer, A. Boca, C. W. Chou, L. M. Duan, and H. J. Kimble, *Nature* **423**, 731 (2003).
8. R. Cao, R. Wen, Z. Gu, Z. Han, P. Qian, and J. Chen, *Chin. Opt. Lett.* **14**, 080201 (2016).
9. S. Du, P. Kolchin, C. Belthangady, G. Y. Yin, and S. E. Harris, *Phys. Rev. Lett.* **100**, 183603 (2008).
10. Z. Han, P. Qian, L. Zhou, J. F. Chen, and W. Zhang, *Sci. Rep.* **5**, 9126 (2015).
11. J. F. Chen, S. Zhang, H. Yan, M. M. T. Loy, G. K. L. Wong, and S. Du, *Phys. Rev. Lett.* **104**, 183604 (2010).
12. Y.-W. Cho, K.-K. Park, J. C. Lee, and Y. H. Kim, *J. Korean Phys. Soc.* **63**, 943 (2013).
13. Q. Chen, B. S. Shi, M. Feng, Y. S. Zhang, and G. C. Guo, *Opt. Express* **16**, 21708 (2008).
14. D. S. Ding, Z. Y. Zhou, B. S. Shi, X. B. Zou, and G. C. Guo, *Opt. Express* **20**, 11433 (2012).
15. Y. S. Lee, S. M. Lee, H. Kim, and H. S. Moon, *Opt. Express* **24**, 28083 (2016).
16. C. Shu, P. Chen, T. K. A. Chow, L. Zhu, Y. Xiao, M. M. T. Loy, and S. Du, *Nat. Commun.* **7**, 12783 (2016).
17. L. Zhu, X. Guo, C. Shu, H. Jeong, and S. Du, *Appl. Phys. Lett.* **110**, 161107 (2017).
18. L. Podhora, P. Obšil, I. Straka, M. Ježek, and L. Slodička, *Opt. Express* **25**, 31230 (2017).
19. P. Grangier, G. Roger, and A. Aspect, *Europhys. Lett.* **1**, 173 (1986).
20. J. Su, L. Cui, Y. Li, and X. Li, *Chin. Opt. Lett.* **16**, 041903 (2018).